Journal of Applied Fluid Mechanics, Vol. 18, No. 1, pp. 205-221, 2025.
Available online at www.jafmonline.net, ISSN 1735-3572, EISSN 1735-3645.
https://doi.org/10.47176/jafm.18.1.2701

Numerical Studies on Aerodynamics Performance of Modified Basebleed to Reduce Fuel Consumption in Squareback Cars

M. S. Prasath[1†], C. Sasikumar[2] and G. Sivaraj[3]

[1]*Department of Aeronautical Engineering, Bannari Amman Institute of Technology, Erode, Tamilnadu, 638401, India*
[2]*Department of Mechanical Engineering, Bannari Amman Institute of Technology, Erode, Tamilnadu, 638401, India*
[3]*Subsonic Airflow Testing Facility, Research Park, Bannari Amman Institute of Technology, Erode, Tamilnadu, 638401, India*

†*Corresponding Author Email: prasath.aero@kcgcollege.com*

ABSTRACT

In recent years, the utilization of SUVs (Sport Utility Vehicle) have attracted more in the automobile industry owing to their comfortness, efficient performance and practicality. Since the majority of SUVs are operated over the highway environment, the formation of undesirable aerodynamic drag forces severely affects the performance which leads to increase the fuel consumption. Hence, this paper more focuses to reduce the fuel consumption by introducing a modified basebleed method in the SUV car model. A numerical investigation is performed for SUV car models with modified basebleed and without basebleed for the constant operating speed to examine the aerodynamic parameters such as coefficient of pressure (C_P), coefficient of drag (C_D), coefficient of lift (C_L) and coefficient of side force (C_S) for the varying yaw angle (ψ). The k-ε turbulence model is utilized to predict the pressure field, velocity field and the formation of wake regions over the SUV car models with modified basebleed and without basebleed. The experimental testing is conducted using low speed subsonic wind tunnel to validate the numerical simulation results of car model for the varying velocity. Research witnessed that the fuel consumption rate is reduced to 4.02% for the SUV car model with modified basebleed than without basebleed, based on the reduction in coefficient of drag (C_D). Eventually, the research suggests that implementing modified basebleed at the SUV car model reduces the fuel consumption and aerodynamically supports for better performance.

Article History

Received March 6, 2024
Revised July 3, 2024
Accepted July 24, 2024
Available online November 6, 2024

Keywords:

Basebleed method
Drag reduction
Fuel consumption
Vehicle performance
Passenger car

1. INTRODUCTION

As environmental rules become more rigorous and there is a growing desire for more environmentally friendly transportation options, reducing aerodynamic drag is essential to reduce the fuel consumption and overall performance of passenger cars. However, the demand for utilizing SUVs is rising and simultaneously produces more drag which leads to further increase the fuel consumption. In passenger cars, fuel consumption and drag reduction are related (Vahdati et al., 2018). The majority of the tractive energy used by vehicles, especially at higher speeds is utilized by aerodynamic drag. It emphasizes the need for efficient drag reduction techniques because it directly affects fuel consumption (Futrzynski, 2015). It is widely recognized that reducing aerodynamic drag leads to lower fuel consumption, as demonstrated in recent studies by (Hucho & Sovran, 1993) and (Rose, 1981). Thus, lowering drag can reduce fuel consumption and increase the aerodynamics performance of the vehicles. The significant increases in drag reduction can be achieved from the conventional methods as vehicle body designs continues to change to fulfill the safety and aesthetic criteria. In addition, flow control techniques are widely utilized to reduce aerodynamic drag and it can be adopted in different car body types.

Nath et al. (2021) investigated the aerodynamic flow behaviour using different flow control devices and altered the airflow over/inside the vehicle to lower the formation of drag force. The Vortex Generators (VG) are placed in the flow separation locations to delay the flow separations. Since the SUV's generate larger drag compared to other models, VGs are preferred for SUV type vehicles (Sevilla, 2012). It is observed from the research of (Selvaraju & Parammasivam, 2019) that using the right vortex generator (VG) for a vehicle can reduce drag by up to 9.04% and lower the required power by up to 8.92%. These VGs can be combined with other drag reduction tools like riblets (Yang et al., 2022), and plasma

NOMENCLATURE

A_f	frontal area	D	drag force
C_D	coefficient of drag	L	lift force
C_L	coefficient of lift	S	side force
C_P	coefficient of pressure	f_x	body force in x direction
C_S	coefficient of side force	f_y	body force in y direction
U	vehicle speed	f_z	body force in z direction
FC	Fuel Consumption	φ	slant angle
ψ	yaw angle	H_f	height of basebleed from the ground at the front
B_f	centroid distance of the basebleed at the front	H_r	height of basebleed from the ground at the rear
B_r	centroid distance of the basebleed at the rear		

VG (Hu et al., 2021), to achieve a drag reduction of 14.55%.

The rear portion of the car is equipped with a spoiler to increase negative lift force and decrease drag. According to (Verma et al., 2021), a small passenger vehicle's aerodynamic performance is significantly impacted by the direction of the lip spoiler. The results show that the optimal direction for the lip spoiler is at an angle of 30 degrees, which achieves the least drag force and the greatest negative lift force. At a flow angle of 30 degrees, the combination of a rear spoiler and co-rotating vortex generators can result in a noticeable improvement in static pressure over the car roof, notably at the car rear (Sinhamahapatra et al., 2010). This results in an aerodynamic drag reduction of up to 68.8%, which can enhance the general performance of cars. In addition, side spoilers mounted on a sports car work well and can increase its aerodynamic efficiency (Kurec & Piechna, 2019).

The Active Grille Shutter technology improves automotive engine performance and fuel economy by considering engine room temperature and aerodynamic resistance (El-Sharkawy et al., 2011). The study resulting aerodynamic drag coefficients for Active Grille Shutter openings by simulating important engine room components. According to the findings, lowering the shutter opening can potentially lower fuel consumption by reducing aerodynamic drag. The study also determined the radiator's capacity to dissipate heat and the Active Grille Shutter's ideal opening control curve (Li et al., 2018).

Base flaps are usually used at the trailing portion of the truck to reduce the wake region. Urquhart et al., 2020, reduced the strength of a large-scale rotating structure in the wake by optimizing the design and having a positive flap angle on the downward roof side. This led to a 2% reduction in drag at yaw. Furthermore, in contrast to the 0◦-yaw optimized design, Urquhart and Sebben (2022), concentrated on optimizing trailing edge flaps on a full-scale vehicle utilizing a surrogate model-based method and achieved drag reduction up to 3% at yaw.

The underbody diffusers are commonly used in Formula 1 cars to direct the underbody flow to the rear end of a car. This can be added with other tools also to experience the combined advantage of both drag reduction tools (Nath et al., 2021). These diffusers tend to accelerate the flow by venturi effect (Huminic & Huminic, 2017). (Cooper et al., 2018) compared baseline model with several configurations and found to be the configuration with a 7◦ venturi diffuser equipped with diagonal sealing skirts produced the highest lift coefficient and aerodynamic efficiency. Bayraktar and Bilgili (2018) focused on different Re values and upswept angles of a diffuser on the rear portion of a typical Ahmed body. It has been found that as the angle varies, the reversal zone shifts, and turbulent kinetic energy concentrates in the upper zones.

The basebleed is a system used in artillery shells and bombs to reduce the wake region at the rear ends. This concept can be incorporated in passenger cars (Sivaraj et al., 2018) to energize the flow at the rear end of cars to reduce the wake region. This will eventually reduce the drag generated by up to 6.188% and decreases the fuel consumption of the car (Sivaraj et al., 2023).

The usage of these flow control methods may sound good, but it has their own limitations. Some active flow control methods, such as boundary layer suction, synthetic jets, and plasma actuators, rely on outside power sources to operate, which can increase energy consumption and reduce a vehicle's fuel economy (Sivaraj et al., 2018). Active grille shutters, underbody diffusers, and wheel covers involve moving parts or processes that could increase the complexity and servicing requirements of the vehicle. A few flow control tools include base flaps, rear spoilers, and vortex generators can improve lift (Bayraktar & Bilgili, 2018) or downforce while lowering drag, which can impact a vehicle's stability and handling. The usage of some flow control devices may be illegal in certain regions, as it alters the vehicle’s appearance.

There are small numbers of devices that may be used to increase the aerodynamic efficiency of the vehicle without affecting the aesthetics of the vehicle or violating the law. One such device is basebleed method, which is placed inside the vehicle’s body and does not affect the external aerodynamics of the vehicle. Moreover, this basebleed is an emerging technique with only few researches have been carried out so far, which evident a significant reduction in drag generated and thus decreases the fuel consumption (Al-Saadi, 2018; Irving Brown et al., 2010).

Based on the above necessity, it is important to address the usage of the basebleed approach for passenger cars and it is clearly indicated by the lack of available existing research. Moreover, it is essential to examine the utilization of one such device called basebleed in other car body structures with proper integration method. Only a few researchers have investigated the drag reduction based

on the effect of fuel consumption by basebleed techniques at lower speeds.

Our previous studies have significantly advanced our understanding of basebleed usage in passenger cars. For instance, (Sivaraj et al., 2023) conducted an extensive investigation into drag reduction, revealing the reduction in fuel consumption. Our work laid the foundation for understanding the drag reduction by minimising the wake region at the rear portion of a hatchback car.

Despite these contributions, there remain several unexplored areas that warrant further investigation. In our previous research, we primarily focused on implementing the basebleed in hatchback cars, but did not examine the implementation of the basebleed in square back car models comprehensively. Additionally, the previous research was limited to the usage of single outlet to bleed the air at rear end portion, leaving a gap in understanding how a modified overhead basebleed operates under multiple outlet condition.

To address these gaps, our research aims to implement this modified basebleed. Specifically, we will extend the work of (Sivaraj et al., 2023) by modifying the basebleed design profile. This includes the addition of multiple basebleed outlets at rear end portion of the car which will provide a more comprehensive understanding of the modified basebleed. By doing so, we hope to contribute to a more holistic understanding of drag reduction in passenger cars, and offer new insights into vehicle aerodynamics.

Hence, this research more focuses to investigate the method of implementing the modified basebleed in a car model to improve the aerodynamic performance based on the numerical simulation process. In turn, the coefficient of drag (C_D) analysed with respect to the varying velocity and yaw angles for the car models with and without basebleed to reduce the fuel consumption.

1.1 Aerodynamics of a Car

Vehicle aerodynamics is essential to modern automotive engineering because it has a significant impact on how fuel-efficient, stable, and effective cars are. The goal of aerodynamics research is to analyze and enhance the airflow around a vehicle in order to lower drag and improve performance (Drag α vehicle velocity^2). In recent years, there has been a growing interest in creating more aerodynamic vehicles in an effort to lower emissions and fuel consumption. Drag in a car is generated by many factors like, pressure drag, skin friction drags and rolling resistance. Among them, pressure drag contributes nearly 75% of drag generated by a car (Fabian et al., 2022). As a car moves forward, it experiences aerodynamic forces such as lift (L), drag (D), and side forces along with center of gravity as shown in Fig. 1.

The flow field formation on a car moving forward is a resultant of vehicle aerodynamics (both external and internal) plus other external factors like exhaust gases, and aerodynamic interference from other vehicles. In most of the cases, we consider only the external aerodynamics of the vehicle and concentrate on aerodynamic forces as mentioned above. The external flow around a car creates

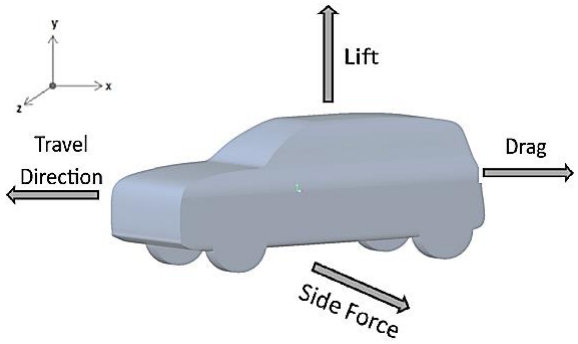

Fig. 1 Aerodynamic forces of a car

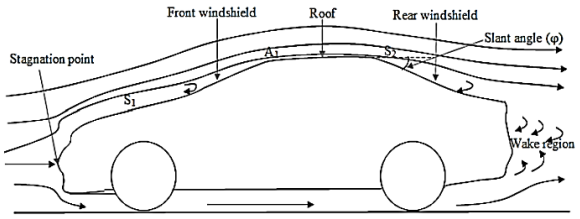

Fig. 2 Schematic flow around a car

velocity vector patterns resulting in the venturi effect (Fig. 2). It is responsible for the pressure and velocity variations on the surface of any car's profile. When the velocity of car increases, the pressure at the front end of car increases and the pressure at the rear end decreases thus creating a wake region at the rear end portion of the car (Wassen & Thiele, 2009).

The moving car experience flow separation and attachments at different locations all over the body of a car. Initially, the flow starts to separate at the bonnet surface (S1) after hitting the front bumper, and later the flow tends to attach (A1) at the end of front windshield, further the flow tends to separate (S2) where the roof ends. This separation (S2) is an important event, where this separation intensity depends on the slant angle (φ) of the vehicle (Peng et al., 2023). This slant angle determines the car body types as hatchback, notchback, fastback and square back.

The force coefficients of the car are calculated with respect to the frontal are with the following expressions (Barnard, 2011).

$$C_D = \frac{D}{\frac{1}{2}\rho U^2 A_f} \tag{1}$$

$$C_L = \frac{L}{\frac{1}{2}\rho U^2 A_f} \tag{2}$$

$$C_S = \frac{S}{\frac{1}{2}\rho U^2 A_f} \tag{3}$$

Where, C_D, C_L and C_S are the coefficients of the respective forces. ρ is the density of the fluid (air); U is the velocity of the car in real-time; A_f is the frontal surface area of the car; Lift (L), Drag (D), and Side force (S) are

directly calculated from the three-component wind tunnel balance.

Among them, the drag generated in a car is nearly 80% of its total resistance when it is travelling above 70km/h. It even increases the fuel consumption of the vehicle, when the car travels at higher speeds. This relation between drag and fuel consumption is expressed as (Himeno & Fujitani, 1993).

$$\frac{\Delta FC}{FC} = \eta \times \left(\frac{\Delta C_D}{C_D} + \frac{\Delta A_f}{A_f} + 3\frac{\Delta U}{U} \right) \quad (4)$$

Where, FC is the fuel consumption of the vehicle; η is property of the driving vehicle which ranges from 0.5 to 0.7 in highway conditions; C_D is drag coefficient; U is the velocity of the car in real-time.

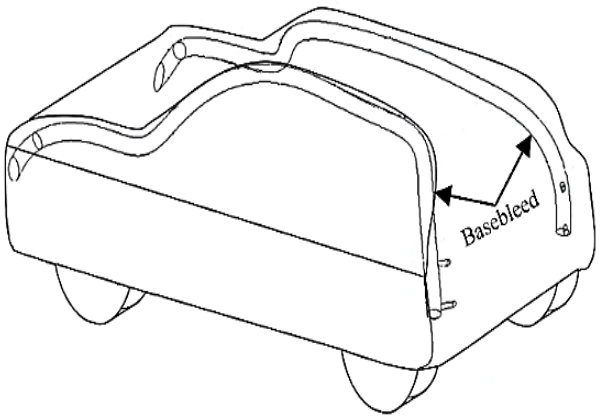

Fig. 3 Modified Basebleed design with one inlet and two outlets

2. MODIFIED BASEBLEED

The basebleed technique involves carefully bleeding high-pressure gas at the back of a vehicle, and it was designed largely for aerospace applications (Serdarevic-Kadic & Terzic, 2019; Molchanov & Siluyanova, 2022). By changing the wake region's flow characteristics, this approach successfully lowers the base pressure and the resulting drag. The principles of basebleed in supersonic and hypersonic flight have been thoroughly investigated by researchers, leading to notable wave drag reductions and improvements in total vehicle performance (Carbajosa et al., 2022; Hu Zhang et al., 2020).

Compared to aerospace uses, the implementations of the concept of basebleed methods in automobile for reducing drag have received less attention throughout the years. Only few researchers have investigated the use of passive bleeding techniques like slotted base flaps. But in the context of passenger cars, the employment of this basebleed system, as seen in aerospace, has gotten barely any attention. It is still possible to develop a modified basebleed techniques for road vehicles that are similar to those used in aerospace applications.

The basebleed method has proven to be efficient in aerospace, but applying it to passenger cars presents special difficulties. Passenger cars travel at lower speeds than aircraft, have different road conditions, and are subject to distinct design limitations. It is important to carefully evaluate the aspects such system complexity, aerodynamic stability, the effect on vehicle dynamics, and the manufacturing feasibility when integrating a modified basebleed system into a car. Additionally, the cost-effectiveness of installing such a system must be assessed in the context of the automotive industry.

For this study, a total of four different models square back car models is used. 'Model 1' is a simple square back model which is named as 'Base model'. Later the car models are modified with basebleed attachments ranging from one outlet to three outlets. For the convenience, these modified models are named as 'Case 1', 'Case 2' and 'Case 3' throughout the study.

The arrangement of these basebleed locations is derived from the optimised basebleed locations by (Sivaraj et al., 2021). The centroid distance of the basebleed at the front is taken as B_f and the basebleed at the rear is taken as B_r. In the same way, the vertical positions (Height) of this basebleed from the ground at the front and rear are denoted as H_f and H_r respectively. Since this technique can be used in reducing drag for any car model, the distance and height of the basebleed locations can be represented as ratios concerning the breadth and height of the car model. To utilize the flow, the basebleed outlets are to be projected to 45^0 angles at the rear end portion of the car. In addition, the centroid distance of each outlet differs from the configuration used e.g., for a two outlet model the distance between the centres of each outlet is 110 mm whereas, for the three-outlet configuration, the distance between the centres of each outlet is 60 mm each. For the single-outlet model, the outlet is positioned at the centre portion at the rear end portion of the car model.

Table 1 Dimensions of Modified Basebleed Configuration

Specification	Case 1	Case 2	Case 3
Diameter of the frontal cross-section of basebleed	100 mm	100 mm	100 mm
Area of the frontal cross-section of basebleed	7853.98 mm^2	7853.98 mm^2	7853.98 mm^2
Diameter of the rear cross-section of basebleed	60 mm	30+30 mm	20+20+20 mm
Area of the rear cross-section of basebleed	2827.43 mm^2	2827.43 mm^2	2827.43 mm^2
Total number of tubes	2 (Numbers)	2 (Numbers)	2 (Numbers)
Total number of outlets	1 (Each)	2 (Each)	3 (Each)
Distance between the centres of each outlet	-	110 mm	60 mm

Table 2 Model specification comparison

Length (mm)	Width (mm)	Height (mm)	Ground Clearance (mm)	Wheel Base (mm)
3995	1800	1620	190	2550

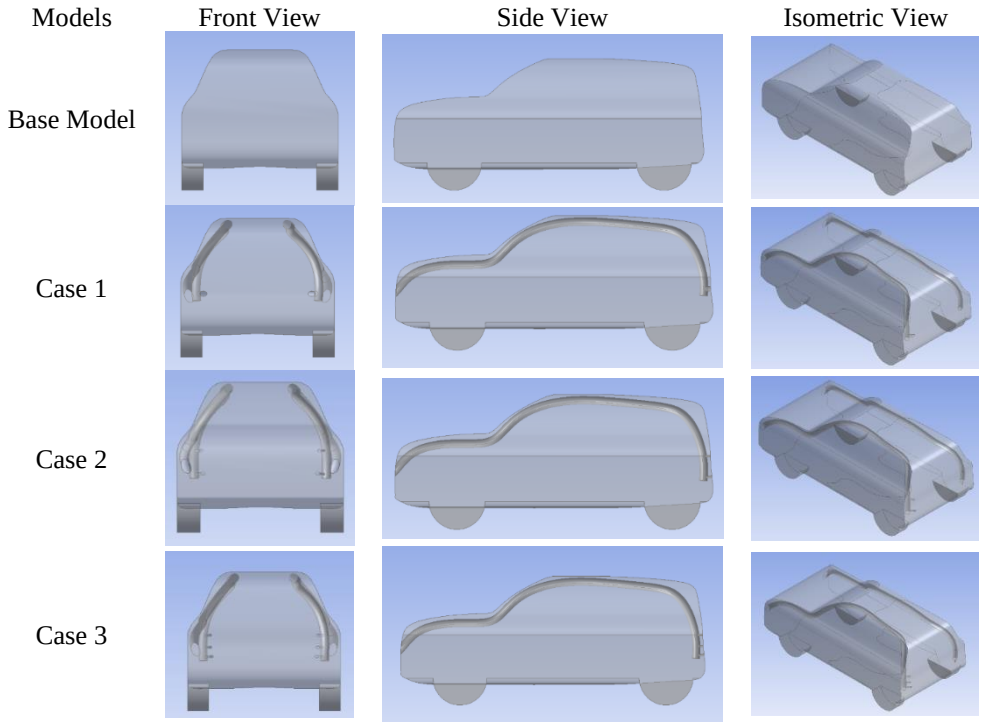

Fig. 4 Different views of Squareback car models

3. NUMERICAL SIMULATION

In vehicle aerodynamics applications, fluid flow optimization is essential for reducing drag. The purpose of this study is to improve aerodynamic efficiency and reduce fuel consumption by examining the possibility of reducing drag in square back car models using Computational Fluid Dynamics (CFD) simulations. The CFD simulation helps us to visualise the flow around the vehicle and study the flow parameters occurring on the vehicle. The CFD simulations are conducted using ANSYS FLUENT for its ability to handle complex geometries using Reynolds-averaged Navier–Stokes (RANS) equations.

3.1 Geometrical Description

The car model chosen for the analysis is a sub 4 metre, Squareback compact SUV, since it is the popular choice of cars in Indian automobile market. The dimensions of the car model are based on some of the popular compact SUVs available in market as shown in the Table 2.

Based on the above considerations shown in Table 1 & Table 2, the dimensions of the SUV model are chosen and designed using CREO Parametric software, feature rich Computer-Aided Designing (CAD) software.

The Fig. 4 shows the three-view diagram of the solid model with and without the modified basebleed. The car model was designed as per the original dimensions mentioned in the Table 2 and later it was scaled down to 1:16 ratio for the meshing and analysis purposes. The length, width and height of the car model are 249.68 mm, 112.5 mm and 101.25 mm respectively. The origin of the domain and car model is set to be at the front portion of the bonnet.

The dimensions of the domain size were normalized with the length of the car L. In consideration with certain parameters like blockage ratio, ground effect, circulation, the domain size was kept as 8L x 3L x 3L (Fig. 5), so that the boundary conditions do not have any unintended effect on the solution. The model was placed at the location of 3L from the inlet so that there is enough space for studying the effect at the rear end of the car.

3.2 Meshing

As part of the Finite Volume Method (FVM) technique, the entire domain was discretized into multiple

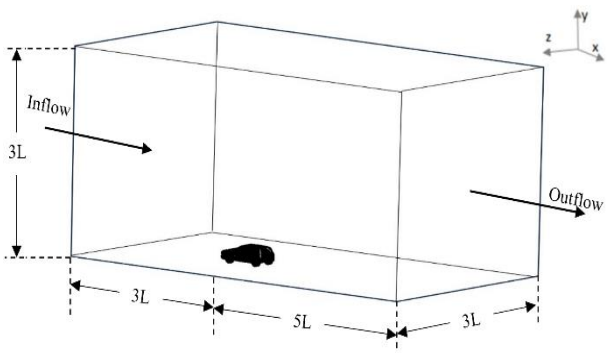

Fig. 5 Computational Domain Specification

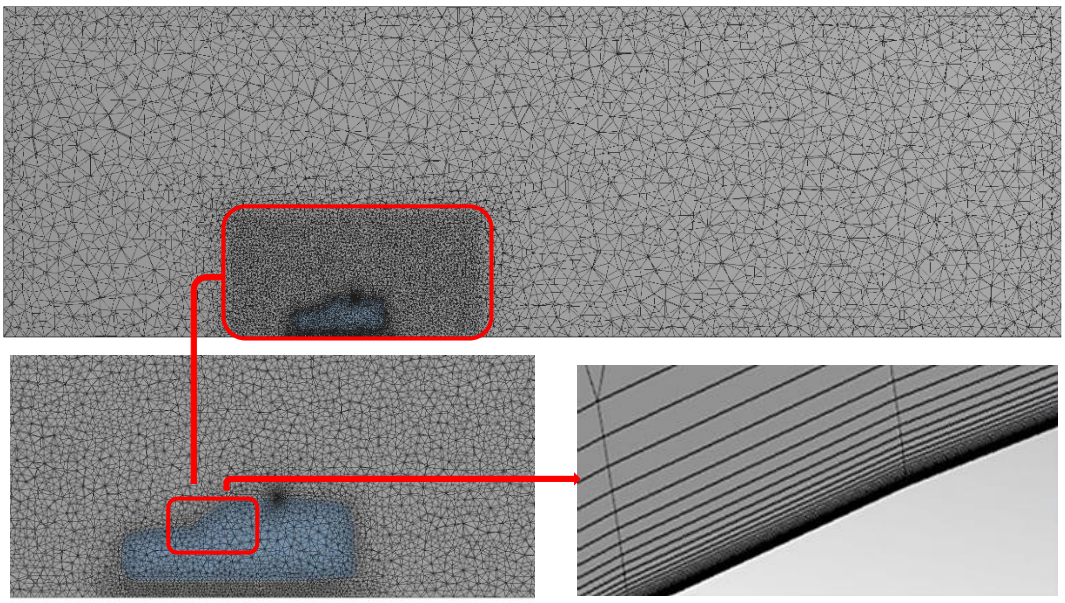

Fig. 6 Unstructured Grid generation for numerical study

numbers of smaller volumes using ANSYS Design Modeller. Unstructured meshing with hexahedral elements was chosen primarily for the volume of the domain. A coarser mesh was constructed at the domain's non-contact regions and a finer mesh was constructed surrounding the car model in order to capture the effects on the model's surface (Wang et al., 2014).

In CFD, accurate modelling of turbulent flows is essential for understanding vehicle aerodynamics, with particular attention paid to the y+ value for capturing boundary layer effects. (Pope, 2000) stresses the significance of precisely resolving the boundary layer, advocating for maintaining appropriate y+ values to ensure accurate near-wall treatment in turbulence models. He suggests that for high-fidelity simulations, y+ should typically remain below 1 to capture the viscous sublayer effectively, while values between 30 and 300 are deemed acceptable for wall-function-based models.

Expanding on these insights, (Spalart, 2015; Igali et al., 2019;) delve deeper into the importance of the y+ value. Spalart emphasizes the necessity of meticulous y+ management to uphold model accuracy, while Zhang et al. highlight its critical role in achieving dependable aerodynamic predictions. Notably, they find that for models like k-ε, maintaining y+ values between 30 and 300 proves crucial for precisely capturing near-wall turbulence and flow separation. Collectively, these findings underscore the y+ value's significance in CFD simulations, directly impacting the reliability of aerodynamic performance evaluations. From these observations, a 10-layer prism mesh was formed around the car with a y+ value of 30 and the first layer thickness of 0.4 mm with a growth rate of 1.2 using the wall function. As a result, a fine mesh with a minimum size of 1.9mm and a total of 4476943 cells was obtained for the computational domain (Fig. 6).

The Reynolds-Averaged Navier-Stokes (RANS) method is widely used in computational fluid dynamics (CFD) for its balance of computational efficiency and accuracy in predicting turbulent flows, particularly in automotive aerodynamics. In automotive aerodynamics, choosing the right turbulence model within the RANS framework is vital for accurately predicting flow characteristics and aerodynamic forces. (Pope, 2000) outlines the fundamental principles of turbulence and the utility of RANS in simplifying the Navier-Stokes equations through averaging, making it a practical choice for many applications.

The Reynolds-Averaged Navier-Stokes (RANS) models, specifically the k-ε, k-ω, and k-ω SST models, are essential tools in computational fluid dynamics (CFD) for simulating turbulent flows due to their balance of accuracy and computational efficiency. The k-ε model, developed by (Jones & Launder, 1972), is widely used for its robustness but struggles with anisotropic flows (Jones & Launder, 1972; Yakhot & Orszag, 1986; Shih et al., 1995). The k-ω model by (Wilcox, 1988) offers improved near-wall predictions but can be sensitive to free-stream turbulence (Wilcox, 1988; Menter, 1994). To address these limitations, (Menter, 1994) introduced the k-ω SST model, which blends the strengths of the k-ϵ and k-ω models, enhancing performance in adverse pressure gradients and separating flows (Menter, 1994; Menter et al., 2014). These models' effectiveness in various engineering applications underscores the importance of choosing the right model based on specific flow characteristics.

Reynolds-Averaged Navier-Stokes (RANS) based turbulence models are used for this flow simulation and the two equation models like *k-ε*, *k-ω* and *SST* models were considered (Gao et al., 2017). The *k-ε* model uses two additional transport equations namely Turbulent Kinetic Energy (TKE) which is denoted by *k* and TKE dissipation rate denoted by *ε* (Mishra & Aharwal, 2018). The Standard *k-ε* (SKE) model was neglected as it may predict large TKE at stagnation point at the flow, so the flow simulation was carried out with the Realizable *k-ε*

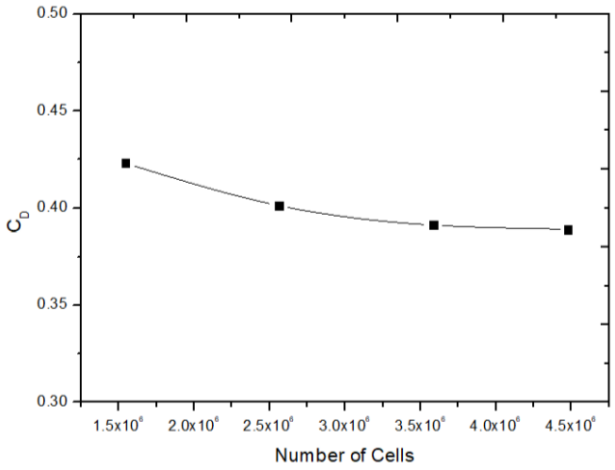

Fig. 7 C_D graph for different Mesh sizes followed for GIS

(RKE) turbulence model in spite of using other turbulence models (Hami, 2021). In addition, the RKE model is suitable for capturing the downstream flow which passes over the rearward region of the car model and the results obtained are satisfactory in near accurate results when used for car models (Altaf et al., 2014). The *k-ω* and *SST* models are suitable for low Reynolds number problems with no wall function, so the y+ values of *k-ω* and *SST* models needs to be lower as 2 and the order of 1 (1-9). Hence the *k-ε* model is an obvious choice of turbulence model selection (Zhang et al., 2019).

Grid Independence Study (GIS) is an inevitable step in a simulation process as this GIS justifies the mesh selection which is used for the entire simulation process. Since, this research mainly focuses on reducing the Drag coefficient C_D, the CD was taken as a primary parameter in GIS. A total of four meshing was generated for this GIS namely Mesh 1, Mesh 2, Mesh 3 and Mesh 4 where the mesh quality was varied from coarser mesh to fine meshes with cell size of 1544668, 2564666, 3583777 and 4476943 respectively (Fig. 7). The C_D was found for the Squareback car model with different mesh sizes and plotted in a graph as shown in Fig. 7 which shows the reduction in drag coefficient C_D (percentage). So, the fine mesh (Mesh 3) with 3583777 cells was used for further carrying out the flow simulation. It has to be noted that selecting a mesh with lesser cells may yield the solution in lesser time, but the quality / accuracy of the solution will be affected by this improper selection of mesh size.

Existing literature and guidelines suggest that such a cell count is adequate for similar aerodynamic studies. For instance, (Tucker, 2001) highlights that a cell counts in the range of 3 to 5 million is generally sufficient for capturing the key aerodynamic characteristics in automotive simulations. Our grid resolution falls well within this range, providing confidence in the robustness of our results. A mesh size of 3583777 is considerably good for the above-mentioned C_D values and this is the choice of meshing for both the models with and without basebleed (Guerrero et al., 2022).

Table 3 Boundary conditions

Solver	Pressure based
Time	Steady state
Turbulence Model	Realizable *k-ε* (RKE)
Operating Condition	101325 Pa
Boundary Conditions	Velocity Inlet – 25 m/s
	Pressure Outlet – 0 Pa
	Wall – Stationary wall
	Ground – Moving wall
Pressure-Velocity Coupling	SIMPLE
Spatial Discretisation	Second order Upwind

3.3 CFD Solver

Based on the Grid Independent Study, the Mesh 3 with 3583777 cells was further used for carrying out the CFD simulations in ANSYS FLUENT, a versatile CFD solver capable of doing simulations with near accurate results when proper boundary conditions were given. The Finite Volume Approach (FVM) approach was used for carrying out the governing equations of fluid mechanics. Continuity, x-, y- and z-momentum equations were considered for the conservation of mass and momentum in the fluid flow (Anderson, 1995).

Continuity equation

$$\nabla \cdot (\rho \cdot U) = 0$$

x- momentum equation

$$\nabla \cdot (\rho \cdot u \cdot U) = -\frac{\partial \mathrm{P}}{\partial x} + \frac{\partial \tau_{\mathrm{xx}}}{\partial x} + \frac{\partial \tau_{\mathrm{yx}}}{\partial y} + \frac{\partial \tau_{\mathrm{zx}}}{\partial z} + \rho f_{\mathrm{x}} \quad (5)$$

y - momentum equation

$$\nabla \cdot (\rho \cdot v \cdot U) = -\frac{\partial \mathrm{P}}{\partial y} + \frac{\partial \tau_{\mathrm{xy}}}{\partial x} + \frac{\partial \tau_{\mathrm{yy}}}{\partial y} + \frac{\partial \tau_{\mathrm{zx}}}{\partial z} + \rho f_{\mathrm{y}} \quad (6)$$

z- momentum equation

$$\nabla \cdot (\rho \cdot w \cdot U) = -\frac{\partial \mathrm{P}}{\partial z} + \frac{\partial \tau_{\mathrm{xy}}}{\partial x} + \frac{\partial \tau_{\mathrm{yx}}}{\partial y} + \frac{\partial \tau_{\mathrm{zz}}}{\partial z} + \rho f_{\mathrm{z}} \quad (7)$$

These three-dimensional governing equations were solved sequentially one after another in an iterative manner with an accuracy of 10^{-6}. The inlet velocity was maintained at 25 m/s which is considered as an average cruising speed of passenger cars at most of the countries and outlet was maintained as a pressure outlet with atmospheric operating conditions. Other than this, all the walls are considered as stationary walls except the bottom face which is ground assumed as moving wall as the boundary conditions for this simulation. (Le Good & Garry, 2004) found that the influence of rotating wheels on drag and lift coefficients is relatively minor compared to other factors such as vehicle body shape and underbody flow. Additionally, (Wäschle, 2007) concluded that the variations in aerodynamic forces due to wheel rotation are negligible when compared to the total aerodynamic forces acting on the vehicle. The inclusion of wheel rotation in our simulations would not significantly alter the outcomes or provide additional insights relevant to the scope of our study (Krajnović & Davidson, 2005). Hence the rotation

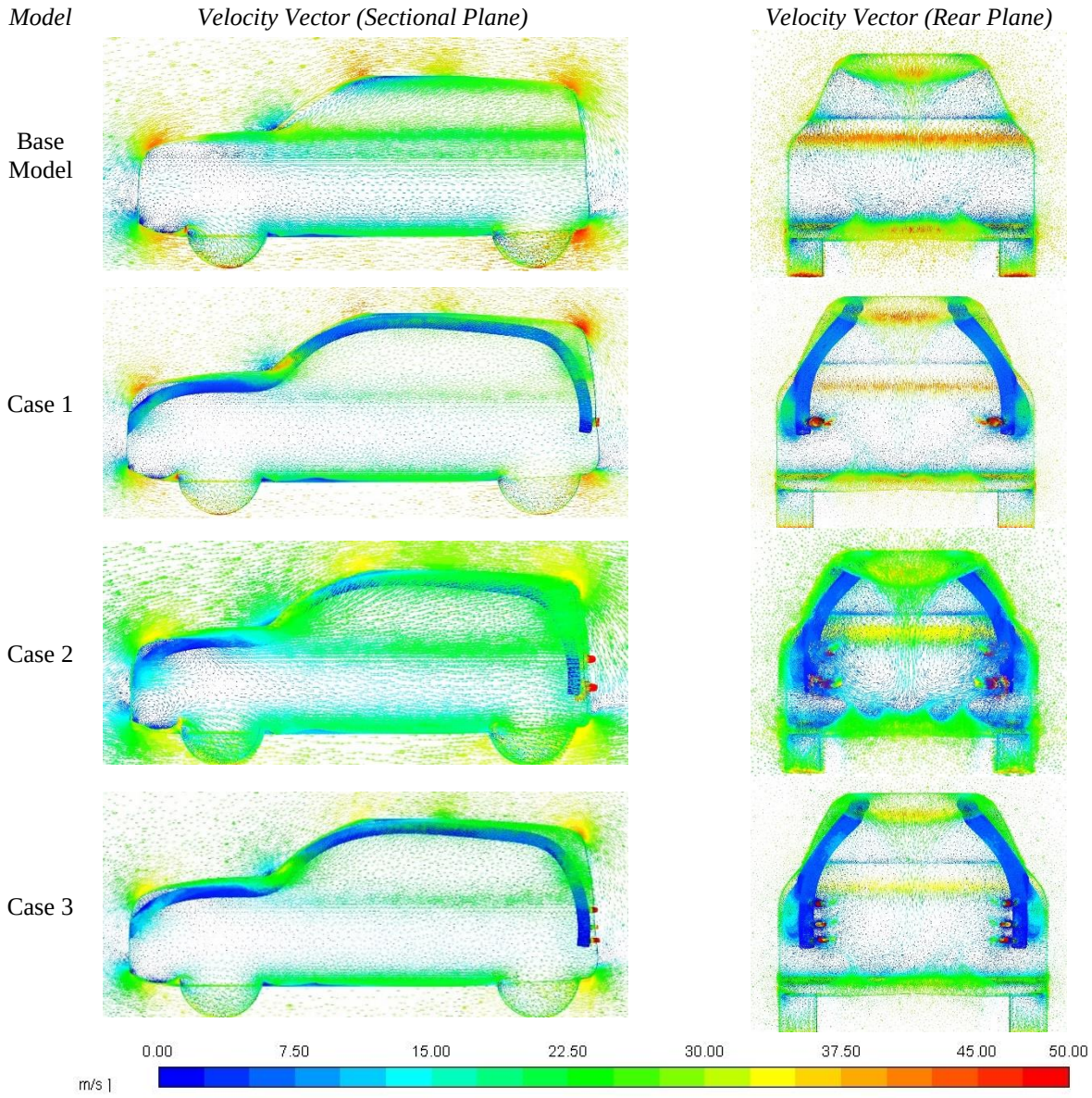

Fig. 8(a) Velocity Vector of car models

is not considered throughout the entire simulation. The pressure - velocity coupling was done with the predictor and corrector method using Semi Implicit Method for pressure Linked Equation (SIMPLE) algorithm. Since RANS equations are used, all the governing equations and other turbulence equations are solved with second order upwind discretization schemes. The convergence criteria for the flow simulation are maintained according to the CFL conditions with convergence accuracy of 10^{-6} for residual and other plots.

The post-processing was carried out in ANSYS CFD POST tool to visualize the three-dimensional flow pattern of airflow around the car models. In addition to that, other flow parameters such as velocity & pressure distribution on the car, lift & drag coefficient, forces and TI are also visualized in terms of contour plots.

4. RESULT AND DISCUSSION

This section presents a comprehensive analysis of the Computational Fluid Dynamics (CFD) simulations conducted on four diverse car models—Base Model, Case1, Case 2 and Case 3. The primary aim of this study was to investigate and compare the intricate aerodynamic performances of these models under varying basebleed conditions such as single outlet, double outlet and three outlets at the rear portion. Through a meticulous examination of velocity distribution, pressure distribution and turbulent intensity, our simulations shed light on the complex flow dynamics surrounding each vehicle.

4.1 Velocity

The three-dimensional flow around the cars is visualized in post processing step. The Fig. 8 shows the velocity vector of fluid flow around the car models with and without the basebleed attached. It is observed that the free stream fluid flow is unaffected until it reaches the front portion of all the car models and gets deflected by the bonnet region. Due to the steep angle at the front, the flow gets stagnated with reduction in velocity and further the flow moves past the bonnet region. A flow separation occurs initially at the bonnet region and later it the flow becomes attached at the front windshield, this attached

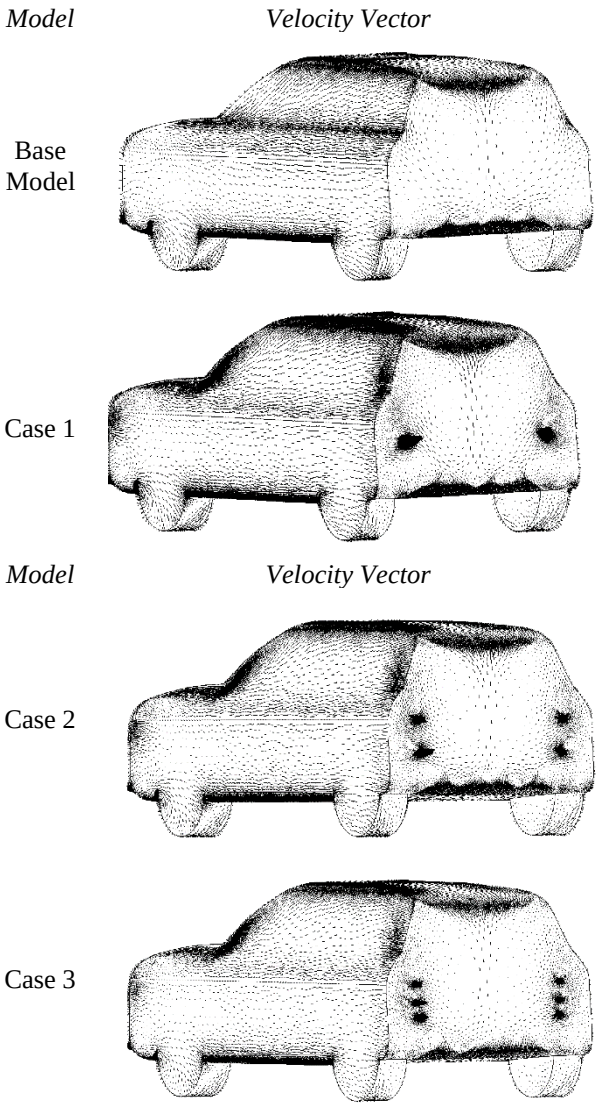

Fig. 8(b) Velocity Vector of car models

flow continues to exist further at the top surface and tends to separate the rear end region at the slant angle. This steep slant angle makes the Squareback vehicles prone to more flow separation at the rear end region which further results in wake region.

This wake region further results in the pressure drag. It is observed that the flow separation and wake region formed at the base model is higher compared to the models with basebleed attached in it. The energized flow from the basebleed exit created desirable flow at the rear end of the vehicle which results in some velocity distributions which eventually minimize the wake region. It is noted that the reduction in wake region results in reducing the drag produced in the entire vehicle. The vortex formation at the rear end is smoother manner in the case 2 model compared to other basebleed models, which can create more vortices at the end portion. This energized flow can be seen in the velocity distribution and pressure formed around the car models as shown in Fig. 9.

Figure 9 illustrates the comparison of velocity profiles of the car models at longitudinal axis. Initially the free stream velocity is maintained at 25 m/s, which is the average cruise speed condition of passenger cars at most

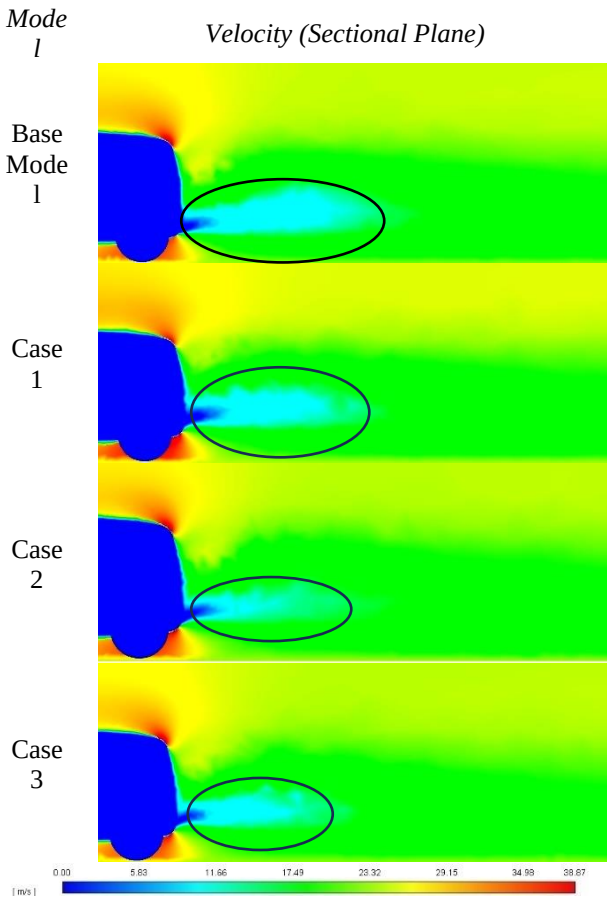

Fig. 9 Velocity distribution at centre plane

of the countries. Similar to the velocity vector profile (Fig. 8), the free stream velocity is stagnated at the front of the car and accelerated at the bonnet region. Due to the flow separation at wind shield, the velocity is reduced and further the flow reattached at the roof surface while reaching maximum velocity up to 38.5m/s as local velocity.

The velocity at the rear end portions of car models differs from each other as the high momentum air reaches rear in models which utilizes the basebleed. It is evident that the base model has comparatively maximum region of low velocity profile observed at the rear end than the other models. This makes the model more prone to the formation of wake region at the rear resulting in pressure drag. Whereas, the models with basebleed have minimum region of low velocity profile observed at the rearward region tends to reduce the formation of wake and pressure drag. Further it is found that case 3 has achieved the higher momentum of energised flow at the rear section of cars comparing to case 1 and case 2 which can be seen further in Fig. 10.

Figure 10 represents a detailed comparison of velocity distributions in car models at different longitudinal planes at the rear end region. Hence six longitudinal planes are located to study the velocity profile at the downstream flow region of the car model. The plane locations down the domain are expressed in terms of length of the car L. The first location is positioned at the extreme closer to the rearend portion of the car model. Further all the other locations are equally spaced between the distance of 0.3 m

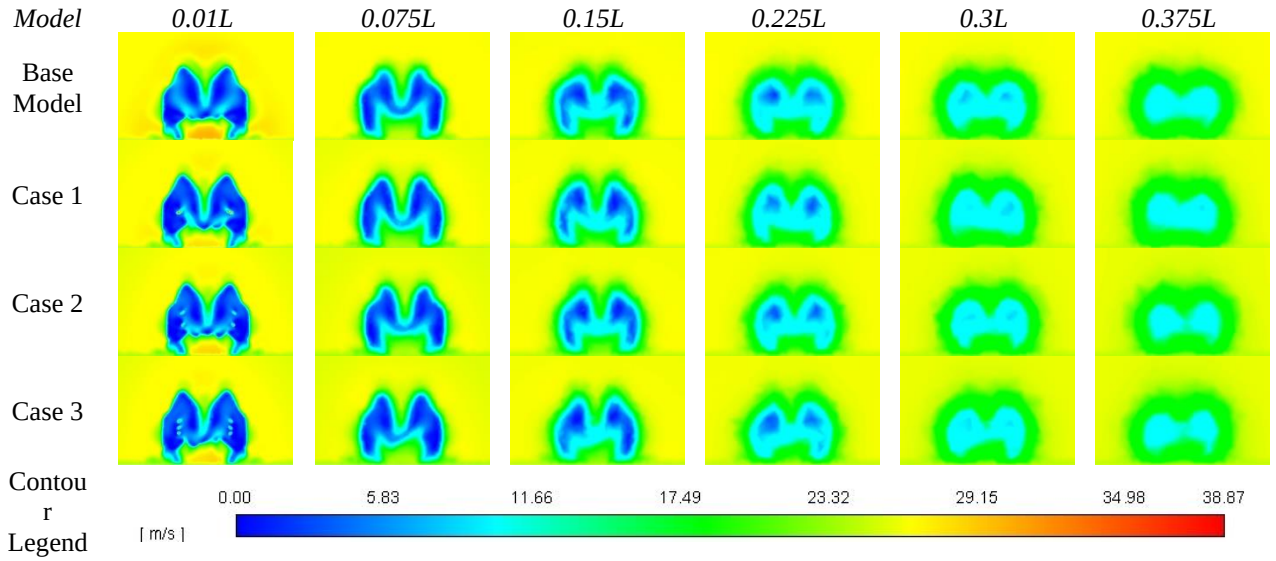

Fig. 10 Velocity distribution along the locations

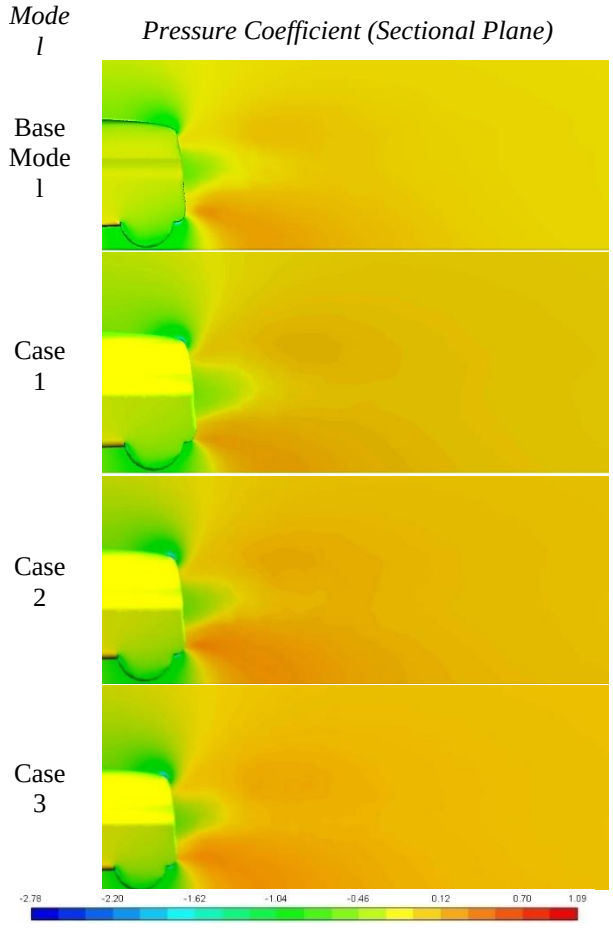

Fig. 11 C_P distribution in center plane

to accurately visualize the flow patterns around the car models. It clearly shows the basebleed has a positive effect in creating momentum at the rear end and it has effect further down the plane. However, this increase in velocity is observed up to 0.225L. This ensures that a car attached with the basebleed does not affect the flow field region of an upcoming car. In case 1, the velocity distribution seems to be uniform up to the 0.225L and the flow became uneven after 0.3L making uneven vortex flow after that plane. The similar uneven velocity distribution can be seen in case 3 from 0.075L making it to cause more turbulence effect at the rear. But in case 2, the velocity distribution is smooth in almost all the planes and the downstream flow is evenly distributed all the way compared to the other models.

4.2 PRESSURE

The pressure distributions on the models are portrayed as Coefficient of Pressure (C_P) distributions over the surface of the cars as mid plane views in Fig. 11.

The pressure coefficient, denoted as *Cp*, is a dimensionless metric that indicates the relative pressure within a fluid flow field. It is defined by the equation,

$$C_P = \frac{p - p_\infty}{\frac{1}{2}\rho V_\infty^2}$$

where:

- p represents the static pressure at a specific point.
- p_∞ is the static pressure in the undisturbed far-field region.
- ρ is the density of the fluid.
- V_∞ is the velocity of the fluid in the free stream.

The C_P distribution on the car surface is same and unaffected in all the models till the flow reaches the rear end. When the flow reaches the rear end region of the car, there is an immediate and significant rise in pressure distribution due to the high energy momentum flow emerged from the basebleed. This can be clearly seen in the C_P distribution on the car models as isometric views in Fig. 12.

Due to the colliding effect in the flows emerging from the basebleed, the rear end portion of the car experiences higher pressure than the model without basebleed. This further clarifies the reduction of wake region at the rear portion by creating high pressure in the downstream of the flow.

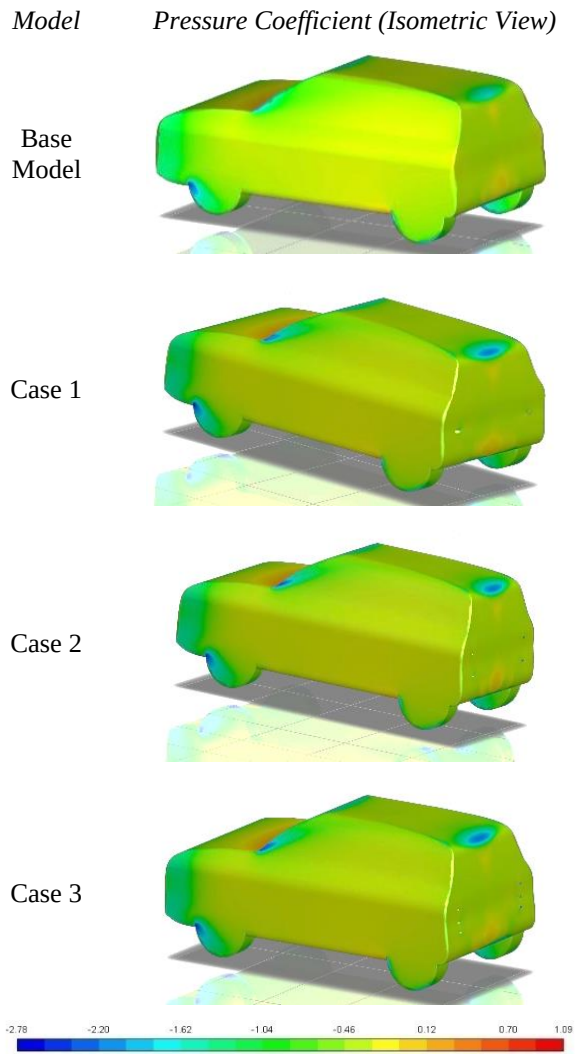

Fig. 12 C_P distribution over the car models

Similar to the velocity profile, the C_P distribution also has immediate effects at the rear portion which is shown in Fig.13. This detailed comparison of the velocity profile shows a significant increase in pressure distribution at the rear end portion of cars with basebleed attached to it. This increase in pressure is experienced immediately downstream of the flow and it extends up to 0.15L. After that the flow is normalised and the pressure becomes ineffective, which proves that installing a basebleed in a car does not affect the free stream flow of an incoming car.

It is evident that from Fig.13 there is a pressure rise in models with basebleed installed and this can be experienced till the third plane. In case 1 and case 2, the pressure is rising gradually till 0.15L and after that the pressure is normalised with the flow field around it. In case 3 the pressure distribution is uneven and this leads to a disturbed flow similar to the one in velocity profile. The quality of the C_P distribution obtained is supported by the given plot Fig.13 which explains the effect of C_P in models with and without basebleed installed.

In addition, the coefficient of pressure distribution over the base model (without basebleed) and with basebleed (Case 1, Case 2, Case 3) are presented in Fig. 14. In order to predict the accuracy of results, the coefficient of pressure value is utilized with forty impinged points over the profile of the car models. It was noted from Fig. 14 that the change in magnitude of pressure distribution is observed at the rear end of the car models attached with and without basebleed devices.

Between the profile points 30 to 40, the formation of pressure coefficient reached the maximum value for the base model without basebleed which is shown in Fig.14(a). In Case 1, the coefficient of pressure slightly reduced between the profile points 30 to 40 due to the attachment of basebleed with single outlet compared to base model [Fig. 14(b)]. Since the basebleed device is designed with two outlets (Case 2), considerably a major reduction in coefficient of pressure is witnessed compared to Case 1. Though a negligible increment in coefficient of pressure observed at profile point 33, further a smooth reduction in the coefficient of pressure observed over the profile points ranges between 30 to 40 which is studied in Fig. 14(c).

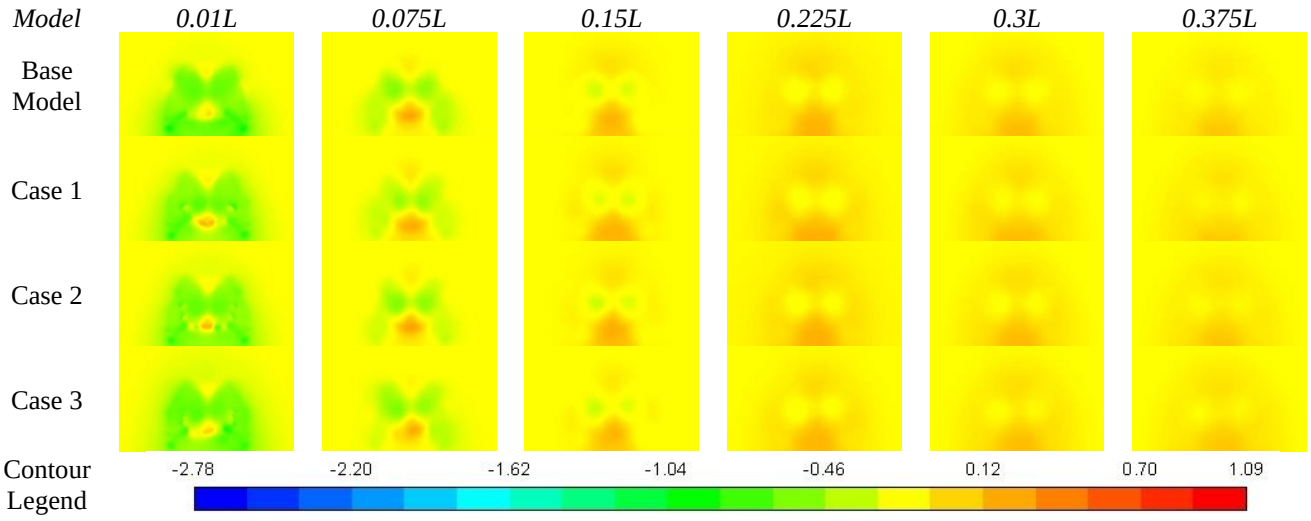

Fig. 13 C_P distribution along the locations

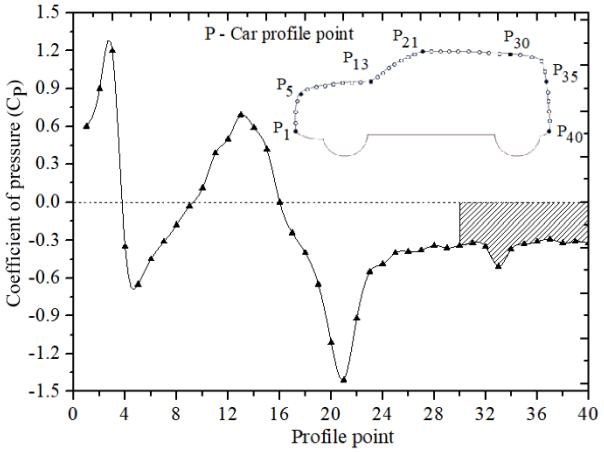

Fig. 14(a) C_P distribution on Base model

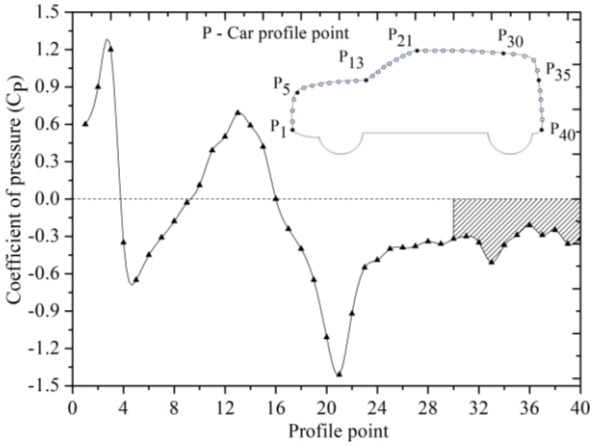

Fig. 14(b) C_P distribution on Case 1 model

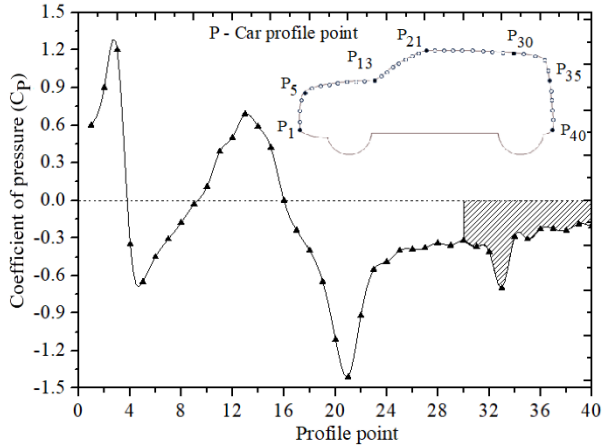

Fig. 14(c) C_P distribution on Case 2 model

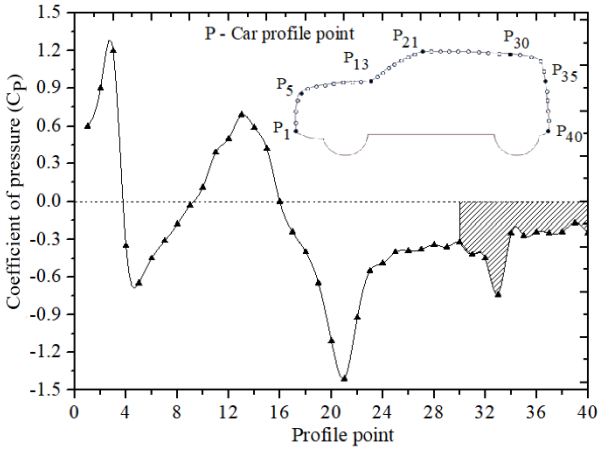

Fig. 14(d) C_P distribution on Case 3 model

At Case 3, gradual decrement in coefficient of pressure studied between the profile points 30 to 40 compared to case 2 [Fig.14(d)]. However, the formation of wake turbulence at the exit of flow field of three outlet basebleed structure (Case 3) causes and undesirable coefficient of drag which affects the performance of the car model. Hence, the coefficient of pressure value noticed at Case 3 is slightly higher than Case 1 & Case 2 for the basebleed device attached with single and double outlets. In addition, the influence of coefficient of pressure observed at the rearward region of Case 2 is -0.192 with reduced coefficient of drag (C_D) = 0.364.

4.3 TURBULENCE

The results of the CFD simulations reveal crucial insights into the turbulent intensity characteristics exhibited by four the car models. It is evident that the base model has a higher turbulence at the rear portion of the car making more vortices and disturbance resulting in increased drag generation. Whereas, the models with basebleed attached as significant changes in turbulence intensity. Due to a single outlet, there is an increased mass flow in case 1, which makes higher turbulence intensity at the exit region of basebleed (Fig. 15). However, this concentration is reduced in case 2 & case 3 and this can be witnessed in Fig. 15 as there is a reduced turbulence field at the downstream. From this comparison, case 2 has a minimum turbulence field at the rear end side ensuring that the installation of this basebleed does not affect the upcoming car at the behind.

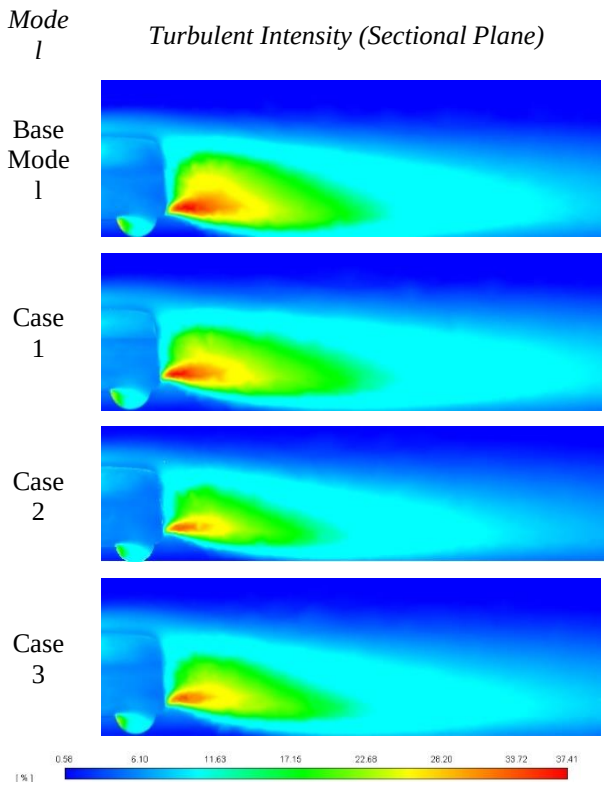

Fig. 15 Turbulent Intensity distribution at the mid plane

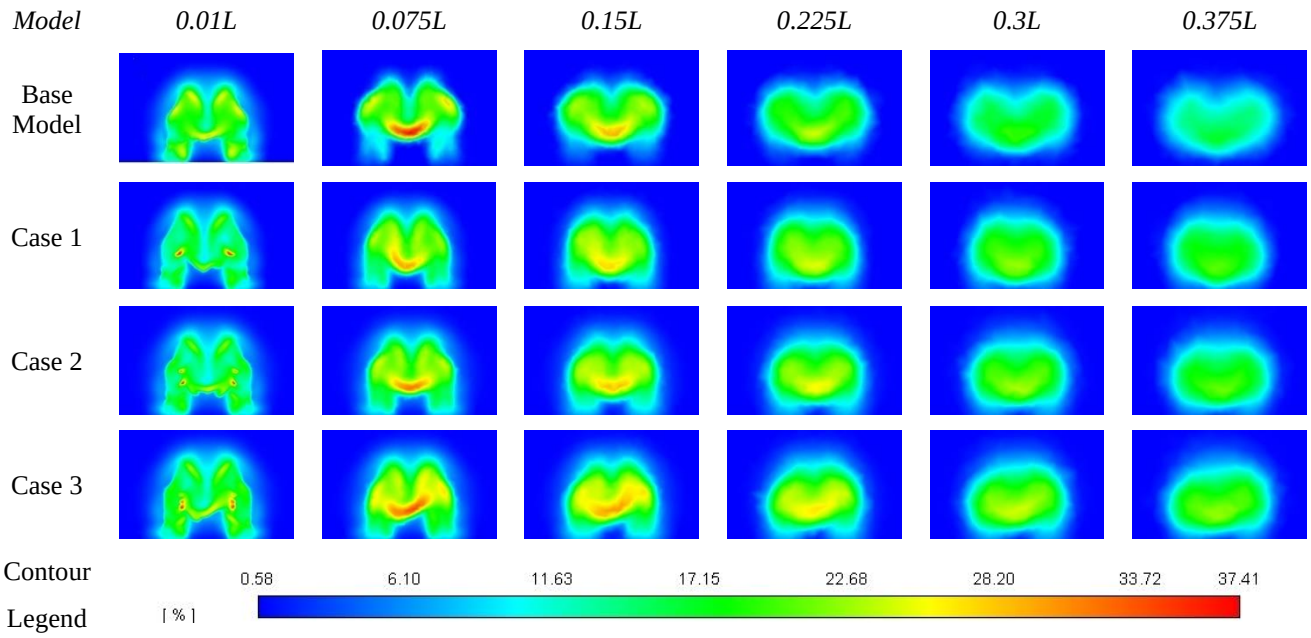

Fig. 16 Turbulent Intensity distribution along the locations

To provide a comprehensive understanding of the turbulent intensity characteristics, a comparative analysis was conducted among the four models. Figure 16 illustrates the relative performance of each model at different rear end planes, emphasizing distinctions in turbulent intensity. The observed variations in turbulent intensity among the car models can be attributed to differences in the interaction of the flow at the rear end region. The comparison gives an insight about the flow behaviour at the rear end of cars and the base model has higher turbulence flow around the vehicle.

In base model, there is an increase in turbulence which can be seen at 0.075L and the turbulence is extended along the width of the car model. This increase in turbulence extends up to 0.225L and then it starts to reduce till 0.375L with minimum flow making wake region at the top & bottom portions of the plane. But in other models, the increase in intensity can be seen at the basebleed exits at the first plane itself. Also, the turbulence formation at the side (along the width is reduced) is reduced due to the high energy flow caused by the basebleed at the rear end region. The increase in turbulence intensity can be seen from the first plane and it extends all the way down to 0.375L. This ensures the presence of high energy flow field at the rear region of car with reduction in the wake region formation. Further this phenomenon resulting in increased pressure behind the vehicle with reduction in overall drag produced. It is evident that the flow field in case 1 & case 3 seems to be disturbed / uneven and this might result in increased vortex formation behind the vehicle. This downstream flow in case 1 & case 3 might cause a disturbed flow for the vehicles that are coming behind. But in case 2, the turbulence distribution is smooth in almost all the planes and the downstream flow is evenly distributed all the way compared to the other models.

These results suggest that the aerodynamic performance of each car model significantly influences the turbulence levels experienced in driving scenarios. The findings of this study carry implications for optimizing vehicle designs to achieve desired turbulent intensity levels.

The variations of angle (ψ) with respect to coefficient of drag (C_D), coefficient of lift (C_L) and coefficient of side force (C_S) are shown in Fig. 17 to19 that indicates the necessity of implementing the basebleed in the SUV car models. Basebleed reduced the coefficient of drag (C_D) and coefficient of side force (C_S) for all the yaw angles compared to the car model without basebleed is observed clearly in Fig. 18 & 19. In addition, the variation of coefficient of lift (C_L) is considerably very minimum and it is negligible for the car models with and without basebleed. However, it is clearly studied that the lift and side forces are reduced whereas the stability of the car model is not affected with basebleed implementation (Fig. 17). Since a minor reduction in coefficient of drag achieved by 6.45% for Case 1 at ψ = 0° whereas Case 2 reached 8.04% for the same yaw angle. Further the desirable flow patterns observed at the rearward region of the car model (Case 2) due to the implementation of two outlet basebleed device. Compared to Case 2, considerably similar reduction in coefficient of drag is observed for Case 3 whereas the rate of increment in coefficient of drag increases with increasing in yaw angle which is found from Fig. 18. At Case 3 imbalanced turbulence wakes formed at the rear section which produces increment in coefficient of drag (C_D) and affects the aerodynamic performance of the car model for the varying yaw angle over Case 2.

In order to validate the computational results, a comparative study was carried out with experimental testing and existing research (Sivaraj et al., 2018). The experimental test was conducted using an open circuit subsonic wind tunnel for the varying velocity (10 m/s to 35 m/s) to study the variations of coefficient drag (CD) for the car models (Base model and Case 2). The preliminary

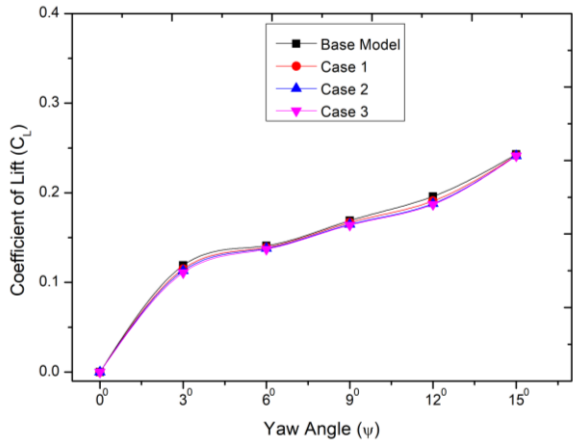

Fig. 17 Comparison of C_L on car models with and without basebleed for various yaw angle

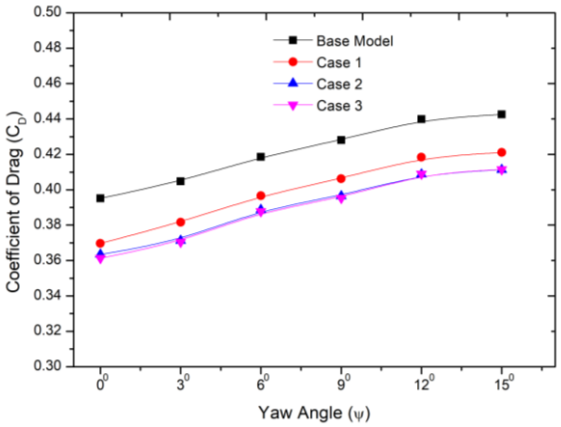

Fig. 18 Comparison of C_D on car models with and without basebleed for various yaw angle

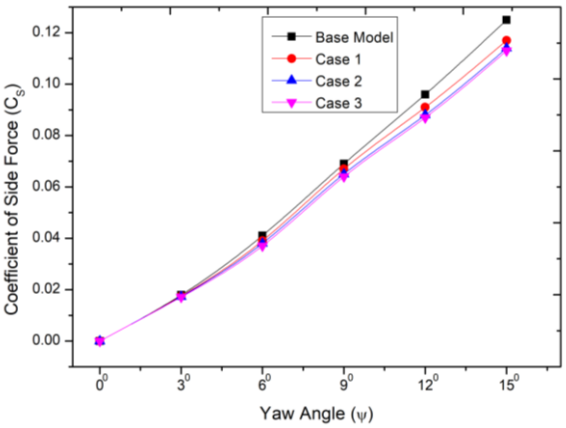

Fig. 19 Comparison of C_S on car models with and without basebleed for various yaw angle

Fig. 19 Experimental Setup

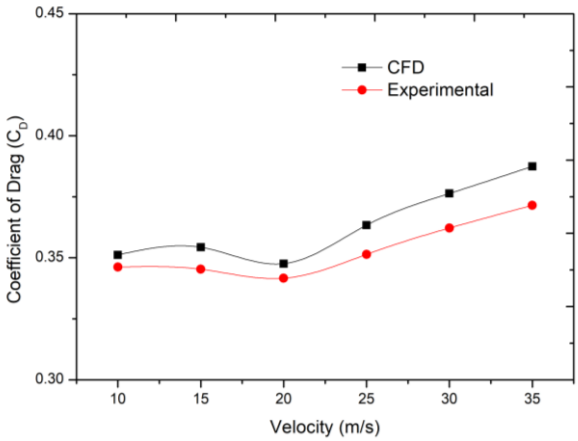

Fig. 20 Comparison of C_D obtained from experimental and numerical studies for Case 2 model

models are fabricated with the scale ratio of 1: 16 based on the geometrical similarity law. The models are placed at the wind tunnel test section area (1.2 m x 0.6 m x 0.6 m) during the experimental process. The experimental test models (0.25m x 0.113m x 0.101m) utilized in this current research are indicated in Fig. 19. The blockage ratio of the model is found to be 3.21% which is within the acceptable limit of 5%. It is a ratio between the area of the projected model to the projected area of the wind tunnel cross-section. The blockage ratio helps to ensure there is no disturbance or backflow inside the test section due to the size of the model. A three-component wind tunnel balance is used to find the aerodynamic forces acting on the model.

The coefficient of drag (C_D) obtained for the varying velocity of car model with basebleed (Case 2) from the computational process, experimental data are compared with existing results are presented in Fig. 20. It was found that the findings show the coefficient of drag (C_D) reached the maximum error percentage of 4.13% and it is witnessed from the computational and experimental results.

The error percentage of coefficient of drag notably reached less than 5% hence the computational and experimental results satisfy the requirement of acceptable operational limit. According to (Martini et al., 2014), discrepancies within a range of 5-10% are generally considered acceptable for aerodynamic studies involving complex flow fields around vehicles. In our study, the differences observed between the numerical simulations and experimental results fall well within this acceptable range. Specifically, the maximum deviation observed was less than 5%, which aligns with the findings reported in the literature. The equation (4) relates the fuel consumption of car model based on the difference of coefficient of drag (C_D) formations. In turn, the researcher (Fred Browand et al., 2007) attained the reduced fuel consumption by 11% for the ratio of reduction in C_D and C_D (ΔC_D/ C_D) of 0.22. (Sivaraj G et al., 2023), arrived the reduction in fuel consumption by 4.3% based on the implementation of basebleed in a hatchback car model for the ratio of reduction in C_D and C_D (ΔC_D/ C_D) of 0.09. Hence this research evident that the reduction in fuel

consumption reached to 4.02% (Case 2) for the ratio of reduction in C_D and C_D (ΔC_D/ C_D) of 0.0804 with two inlets modified basebleed device which is found from the Fig. 20.

5. CONCLUSION

The numerical simulation study was conducted for the car model integrated with and without basebleed to analyse the aerodynamic drag characteristics. The car models with and without basebleed were designed and subjected to computational process for the varying outlet configurations. The velocity field, pressure profile and turbulent intensity around the car models were examined to determine the performance parameters such as coefficient of pressure (C_P), coefficient of drag (C_D), coefficient of lift (C_L) and coefficient of side force (C_S). Further the investigation was extended to validate the numerical simulation results based on the experimental test and existing research. The experimental validation process was conducted using wind tunnel facility with car model (Case 2) for the varying operating speed. The numerical results predicts that the reduction in coefficient of drag (C_D) for Case 2 attained the maximum by 8.04% whereas the fuel consumption reduced to 4.02%. In addition, the coefficient of drag (C_D) attained the minimum value of 0.0804 for the same reduction in fuel consumption which is witnessed for the car model implemented with two inlet basebleed (Case 2). It is suggested that SUV car models integrated with two outlet basebleed predominantly reduced the coefficient of drag (C_D) and improve the vehicle performance with negligible impact on the stability.

ACKNOWLEDGEMENTS

The authors would like to thank the Advanced Computing Facility and Subsonic Airflow Testing Facility, Research Park, Bannari Amman Institute of Technology for their support during the computational analysis.

CONFLICT OF INTEREST

The authors have no conflict of interest to disclose in this research work.

AUTHORS CONTRIBUTION

M. S. Prasath: Developed conceptualization, methodology, Designing and Simulation; **C. Sasikumar:** Performed Writing – oral draft preparation; **G. Sivaraj:** performed writing – validation, reviewing and editing.

REFERENCES

Al-Saadi, (2018). *Analysis of novel techniques of drag reduction and stability increase for sport utility vehicles using computational fluid dynamics*. University of Al-Qadisiyah, February 2019. https://doi.org/10.13140/RG.2.2.15580.74880

Altaf, A., Omar, A. A., & Asrar, W. (2014). Passive drag reduction of square back road vehicles. *Journal of Wind Engineering and Industrial Aerodynamics*, *134*, 30–43. https://doi.org/10.1016/j.jweia.2014.08.006

Anderson, J. D. (1995). *Computational fluid dynamics : the basics with applications*. McGraw-Hill.

Barnard, R. H. (2011). Road vehicle aerodynamic design: an introduction. *The Aeronautical Journal* (Issue 1011). https://doi.org/10.1017/S0001924000065787

Bayraktar, S., & Bilgili, Y. O. (2018). Effects of under body diffuser on the aerodynamics of a generic car. *International Journal of Automotive Engineering and Technologies*, *7*(2), 99–109. https://doi.org/10.18245/ijaet.458901

Carbajosa, C., Martinez-Cava, A., Valero, E., & Paniagua, G. (2022). Efficiency of pulsating base bleeding to control trailing edge flow configurations. *Applied Sciences (Switzerland)*, *12*(13). https://doi.org/10.3390/app12136760

Cooper, K. R., Bertenyi, T., Dutil, G., Syms, J., & Sovran, G. (2018). The Aerodynamic Performance of Automotive Underbody Diffusers. *SAE Technical Paper* 980030, 1998. https://doi.org/10.4271/980030

El-Sharkawy, A. E., Kamrad, J. C., Lounsberry, T. H., Baker, G. L., & Rahman, S. S. (2011). Evaluation of impact of active grille shutter on vehicle thermal management. *SAE International Journal of Materials and Manufacturing*, *4*(1), 1244–1254. https://doi.org/10.4271/2011-01-1172

Fabian, M., Huňady, R., Kupec, F., & Mlaka, T. (2022). Effect of the aerodynamic elements of the hatchback tailgate on the aerodynamic drag of the vehicle. *Advances in Science and Technology Research Journal*, *16*(6), 73–87. https://doi.org/10.12913/22998624/155308

Fred Browand, Rose McCallen, & James Ross. (2007). *The aerodynamics of heavy vehicles II: Trucks, buses, and trains: Vol. II*. Lecture Notes in Applied and Computational Mechanics.

Futrzynski, R. (2015). *Drag reduction using plasma actuators*. Engineering Sciences, KTH Royal Institute of Technology.

Gao, F., Wang, H., & Wang, H. (2017). Comparison of different turbulence models in simulating unsteady flow. *Procedia Engineering*, *205*, 3970–3977. https://doi.org/10.1016/j.proeng.2017.09.856

Guerrero, A., Castilla, R., & Eid, G. (2022). A numerical aerodynamic analysis on the effect of rear underbody diffusers on road cars. *Applied Sciences (Switzerland)*, *12*(8). https://doi.org/10.3390/app12083763

Hami, K. (2021). Turbulence modeling a review for different used methods. *International Journal of Heat and Technology*, *39*(1), 227–234. https://doi.org/10.18280/ijht.390125

Himeno, R., & Fujitani, K. (1993). Numerical analysis and visualization of flow in automobile aerodynamics development. *Journal of Wind Engineering and Industrial Aerodynamics*, 46. https://doi.org/10.1016/0167-6105(93)90354-Q

Hu, X., Zhang, J., Hui, Z., Luo, Y., Guo, P., & Wang, J. (2021). Flow control of automobile with plasma vortex generator. *Journal of Mechanical Science and Technology*, *35*(6), 2493–2502. https://doi.org/10.1007/s12206-021-0520-5

Hucho, W. H., & Sovran, G. (1993). Aerodynamics of road vehicles. *Annual Review of Fluid Mechanics*, *25*, 1993, 25. https://doi.org/10.1146/annurev.fl.25.010193.002413

Huminic, A., & Huminic, G. (2017). Aerodynamic study of a generic car model with wheels and underbody diffuser. *International Journal of Automotive Technology*, *18*(3), 397–404. https://doi.org/10.1007/s12239−017−0040−6

Igali, D., Mukhmetov, O., Zhao, Y., Fok, S. C., & Teh, S. L. (2019). Comparative analysis of turbulence models for automotive aerodynamic simulation and design. *International Journal of Automotive Technology*, *20*(6), 1145–1152. https://doi.org/10.1007/s12239-019-0107-7

Irving Brown, Y. A., Windsor, S., & Gaylard, A. P. (2010). The effect of base bleed and rear cavities on the drag of an SUV. *SAE Technical Papers*. https://doi.org/10.4271/2010-01-0512

Jones, W. P., & Launder, B. E. (1972). The prediction of laminarization with a two-equation model of turbulence. *International Journal of Heat and Mass Transfer*, *15*(2), 301–314. https://doi.org/10.1016/0017-9310(72)90076-2

Krajnović, S., & Davidson, L. (2005). Influence of floor motions in wind tunnels on the aerodynamics of road vehicles. *Journal of Wind Engineering and Industrial Aerodynamics*, *93*(9), 677–696. https://doi.org/10.1016/j.jweia.2005.05.002

Kurec, K., & Piechna, J. (2019). Influence of side spoilers on the aerodynamic properties of a sports car. *Energies*, *12*(24). https://doi.org/10.3390/en12244697

Le Good, G. M., & Garry, K. P. (2004, March 8). *On the use of reference models in automotive aerodynamics*. https://doi.org/10.4271/2004-01-1308

Li, J., Deng, Y., Wang, Y., Su, C., & Liu, X. (2018). CFD-Based research on control strategy of the opening of Active Grille Shutter on automobile. *Case Studies in Thermal Engineering*, *12*, 390–395. https://doi.org/10.1016/j.csite.2018.05.009

Martini, H., Gullberg, P., & Lofdahl, L. (2014). Comparative studies between CFD and wind tunnel measurements of cooling performance and external aerodynamics for a heavy truck. *SAE International Journal of Commercial Vehicles*, *7*(2), 2014-01–2443. https://doi.org/10.4271/2014-01-2443

Menter, F. R. (1994). Two-equation eddy-viscosity turbulence models for engineering applications. *AIAA Journal*, *32*(8), 1598–1605. https://doi.org/10.2514/3.12149

Menter, F., Menter, F. R., Kuntz, M., & Langtry, R. (2014). Ten years of industrial experience with the SST turbulence model. *Turbulence, heat and mass transfer*, 625-632. https://www.researchgate.net/publication/228742295

Mishra, P., & Aharwal, K. R. (2018). *A review on selection of turbulence model for CFD analysis of air flow within a cold storage.* IOP Conference Series: Materials Science and Engineering, 402(1). https://doi.org/10.1088/1757-899X/402/1/012145

Molchanov, A. M., & Siluyanova, M. V. (2022). Numerical investigation of a near-wake flowfield with base bleed. *Journal of Physics: Conference Series*, *2308*(1). https://doi.org/10.1088/1742-6596/2308/1/012011

Nath, D. S., Pujari, P. C., Jain, A., & Rastogi, V. (2021). Drag reduction by application of aerodynamic devices in a race car. *Advances in Aerodynamics*, *3*(1). https://doi.org/10.1186/s42774-020-00054-7

Peng, F., Yan, F., Yin, B. J., & Liang, J. N. (2023). Experimental study on wake characteristics of secondary grooved cylinders with different depths. *Journal of Applied Fluid Mechanics*, *16*(5), 1057–1073. https://doi.org/10.47176/jafm.16.05.1592

Pope, S. B. (2000). *Turbulent flows*. Cambridge University Press. https://doi.org/10.1017/CBO9780511840531

Rose, M. J. (1981). Commercial vehicle fuel economy — The correlation between aerodynamic drag and fuel consumption of a typical truck. *Journal of Wind Engineering and Industrial Aerodynamics*, *9*(1–2), 89–100. https://doi.org/10.1016/0167-6105(81)90080-5

Selvaraju, P. N., & Parammasivam, K. M. (2019). Empirical and numerical analysis of aerodynamic drag on a typical SUV car model at different locations of vortex generator. *Journal of Applied Fluid Mechanics*, *12*(5), 1487–1496. https://doi.org/10.29252/JAFM.12.05.29674

Serdarevic-Kadic, S., & Terzic, J. (2019). *Preliminary design method for base bleed unit* (pp. 055–070). https://doi.org/10.2507/daaam.scibook.2019.05

Sevilla, Y. A. (2012). *Drag reduction of sport utility vehicle using vortex generators.* Master's thesis, California State University. https://hdl.handle.net/10211.9/1780.

Shih, T. H., Liou, W. W., Shabbir, A., Yang, Z., & Zhu, J. (1995). A new k-ϵ eddy viscosity model for high reynolds number turbulent flows. *Computers & Fluids*, *24*(3), 227–238. https://doi.org/10.1016/0045-7930(94)00032-T

Sinhamahapatra, K. P. (2010). *Indian institute of technology kharagpur department of aerospace*

engineering, ICTACEM (5 2010.12.27-29 Kharagpur), & International Conference on Theoretical, A. (2010). Aerodynamic Effects of Rear Spoiler and Vortex Generators on Passenger Cars.

Sivaraj, G., Parammasivam, K. M., & Suganya, G. (2018). Reduction of aerodynamic drag force for reducing fuel consumption in road vehicle using basebleed. *Journal of Applied Fluid Mechanics*, *11*(6), 1489–1495. https://doi.org/10.29252/jafm.11.06.29115

Sivaraj, G., Parammasivam, K. M., Prasath, M. S., & Lakshmanan, D. (2023). Numerical simulation of hatchback car with modified vehicle design for the improvement of fuel consumption. *Journal of Applied Fluid Mechanics*, *16*(9). https://doi.org/10.47176/jafm.16.09.1828

Sivaraj, G., Parammasivam, K. M., Prasath, M. S., Vadivelu, P., & Lakshmanan, D. (2021). Low analysis of rear end body shape of the vehicle for better aerodynamic performance. *Materials Today: Proceedings*, *47*, 2175–2181. https://doi.org/10.1016/j.matpr.2021.05.521

Spalart, P. R. (2015). Philosophies and fallacies in turbulence modeling. *Progress in Aerospace Sciences*, *74*, 1–15. https://doi.org/10.1016/j.paerosci.2014.12.004

Tucker, P. G. (2001). *Computation of unsteady internal flows*. Springer US. https://doi.org/10.1007/978-1-4615-1439-8

Urquhart, M., Varney, M., Sebben, S., & Passmore, M. (2020). Aerodynamic drag improvements on a square-back vehicle at yaw using a tapered cavity and asymmetric flaps. *International Journal of Heat and Fluid Flow*, *86*. https://doi.org/10.1016/j.ijheatfluidflow.2020.108737

Vahdati, M., Beigmoradi, S., & Batooei, A. (2018). Minimising drag coefficient of a hatchback car utilising fractional factorial design algorithm. *European Journal of Computational Mechanics*, *27*(4), 322–341. https://doi.org/10.1080/17797179.2018.1550962

Verma, R. P., Kumar Chaudhary, N., & Avikal, S. (2021). Effect of direction of lip spoiler on the aerodynamic performance of a small passenger vehicle. *Materials Today: Proceedings*, *46*, 10301–10305. https://doi.org/10.1016/j.matpr.2020.12.448

Wang, Y., Xin, Y., Gu, Z., Wang, S., Deng, Y., & Yang, X. (2014). Numerical and experimental investigations on the aerodynamic characteristic of three typical passenger vehicles. *Journal of Applied Fluid Mechanics*, *7*(4), 659–671. https://doi.org/10.36884/jafm.7.04.21460

Wäschle, A. (2007). The Influence of Rotating Wheels on Vehicle Aerodynamics - Numerical and Experimental Investigations. *SAE Technical Paper*, *2007*. https://doi.org/10.4271/2007-01-0107.

Wassen, E., & Thiele, F. (2009). Road vehicle drag reduction by combined steady blowing and suction. *39th AIAA Fluid Dynamics Conference, June 2009*, San Antonio, Texas. http://doi.org/10.2514/6.2009-4174.

Wilcox, D. C. (1988). Reassessment of the scale-determining equation for advanced turbulence models. *AIAA Journal*, *26*(11), 1299–1310. https://doi.org/10.2514/3.10041

Yakhot, V., & Orszag, S. A. (1986). Renormalization-group analysis of turbulence. *Physical Review Letters*, *57*(14), 1722–1724. https://doi.org/10.1103/PhysRevLett.57.1722

Yang, X., Hu, Y., Gong, Z., Jian, J., & Liu, Z. (2022). Numerical study of combined drag reduction bases on vortex generators and riblets for the ahmed body using IDDES methodology. *Journal of Applied Fluid Mechanics*, *15*(1), 193–207. https://doi.org/10.47176/jafm.15.01.32832

Zhang, B. H., Zhao, Y. X., & Liu, J. (2020). Effects of bleed hole size on supersonic boundary layer bleed mass flow rate. *Journal of Zhejiang University: Science A*, *21*(8), 652–662. https://doi.org/10.1631/jzus.A1900507

Zhang, C., Bounds, C. P., Foster, L., & Uddin, M. (2019). Turbulence modeling effects on the CFD predictions of flow over a detailed full-scale sedan vehicle. *Fluids*, *4*(3). https://doi.org/10.3390/fluids4030148